PROCEEDINGS OF SCIENCE

A two-dimensional model for some unusual features of martesites

S. Sreekala[*] [†] **and G. Ananthakrishna**
Materials Research Centre, Indian Institute of Science, Bangalore-560012, India
E-mail: sree@mrc.iisc.ernet.in, garani@mrc.iisc.ernet.in

Here we present a summary of the results of a detailed study of two dimensional model for square-to-rectangle martensitic transformation that explains several unusual features of the martensitic transformation. This model includes inertial effects, dissipation, long-range interaction between the transformed domains and an inhomogeneous stress field to describe the effect of lattice defects which serves as nucleation centers. Studies of single-site and multi-site nucleation cases for single quench situation and thermal cycling show that most results are insensitive to initial distribution of the defects. Thermal cycling using continuous cooling and heating simulations show the existence of hysteresis in the transformation. More importantly, the rate of energy dissipated occurs in the forms of bursts with power law statistics for their amplitudes and durations which explains the results of acoustic emission signals observed in experiments. For the case of thermal cycling in a restricted domain of temperatures, the dissipated bursts of energy are repetitive, a feature observed in experiments. The associated morphology shows a complete reversal of the martensite domains thus throwing light on the mechanism underlying the shape memory effect. The model also exhibits tweed like patterns.

International conference on Statistical Mechanics of Plasticity and Related Instabilities
August 29-September 2, 2005
Indian Institute of Science, Bangalore, India

[*] Speaker.
[†] SS would like to acknowledge JNCSAR, Jakkur, Bangalore for the financial support

PoS(SMPRI2005)056

Contents

1. INTRODUCTION

Martensitic transformation is a first order transition yet it exhibits several features of a second order transition. The pretransitional effect observed as the system approaches the martensitic transformation temperature is an example of critical fluctuation [1, 2, 3, 4]. The associated enhanced levels of fluctuation observed in several measurable quantities (such as the anomalous scattering and tweed structure) has been recorded in a number of different systems [1, 3, 4]. Another example related to acoustic emission (AE) that usually accompanies martensite transformation is the power law distribution of the amplitudes and intervals reported in experiments on Cu-Al-Zn single crystals. Vives *et. al.* [5, 6], reported that the distributions of the amplitudes of the AE signals and their durations obey power law statistics (which implies scale free nature of the underlying process) when the samples were subjected to slow thermal cycling both during cooling and heating runs. However, in this case, as the AE signals are accumulated during thermal cycling, there is no tuning as in second order transition. Thus, it is actually reminiscent of self-organized criticality introduced by Bak *et. al.*, [7]. Another unusual and interesting property of the AE signals reported is the high degree of reproducibility and statistical correlation in time when the system is subjected to repeated thermal cycling over a restricted range of temperatures [8]. The near repetitive nature of AE signals during successive cycles is shown to be correlated with the growth and shrinkage of martensite domains. Thus, exploring this correlated behavior should help us to understand the

shape memory effect as well. Moreover, at a conceptual level, the nature of correlation of the repetitive AE signals is significantly different from the power law nature of the statistics observed during full thermal cycling mentioned above. Thus, it would be desirable to capture the seemingly conflicting properties using a single model.

The martensitic transformations are a class of diffusion-less first order solid-solid structural phase transformations wherein the nearest neighbors in the parent phase remain so in the product phase also. On lowering the temperature, the lattice gets distorted due to spontaneous displacement of the atoms during the transformation from the higher symmetry austenite phase to the lower symmetry martensite phase. This creates long-range strain fields which in turn strongly depend on the relative positions and orientations of the martensitic plates that eventually leaves the system in a metastable state. Thus, the transformation path depends on continuously evolving configurations. Given a fixed quench, and hence a fixed amount of drive, the amount of transformed phase is fixed and further under-cooling would be required to increase the product phase. On cooling, the transformation starts at a temperature M_s, called the martensite start temperature and is completed at a temperature M_f (martensite finish temperature). In the reverse heating cycle, the transformation is initiated at a temperature A_s (austenite start temperature) and ends at a temperature A_f (austenite finish temperature), which in general can be much higher than the martensitic start temperature M_s. The related shape memory effect usually accompanies the transformation. The above features also imply that thermal fluctuations have little role in the transformation kinetics. Such martensites are called athermal.

It is well known that in athermal martensites, nucleation occurs at defect sites like dislocations or grain boundaries [9, 10, 11]. Another interesting feature of these transformations is the auto-catalytic cooperative nature of nucleation [9]. It is observed that a martensite domain that has nucleated from a specific site in the crystal, triggers the nucleation of other domains in the vicinity.

Recently, a simple two dimensional phenomenological model has been shown to capture the power law statistics under thermal cycling [12]. This model attempts to incorporate the essential features of systems evolving to SOC state, namely, slow driving, threshold dynamics, appropriate relaxational mode without any recourse to tuning any relevant parameter. Surprisingly, this model also captures the correlated nature of the AE signals when the system is cycled in a restricted range of temperatures [13, 14], with the associated growth and decay of the martensite domains. The paper summarizes the results of an extensive numerical simulations on this two dimensional model describing square-to-rectangle martensitic transformation [12, 13, 14]. We discuss the results of a single-defect quench, multi-defect quench, thermal cycling over broad range of temperatures, the power law statistics arising in both in single and multi-defect cases, the correlated nature of AE signals and the associated shape memory effect, and finally the tweed like structure.

2. THE MODEL

The basic idea of the model is to include all the important features of athermal martensites such as inertial effects, long- range interaction and dissipation. The inertial effect is included by accounting for finite propagation time [15, 16]. It has been demonstrated that inertial effects prohibit the growth of martensite as a single variant in the presence of dissipation (in one dimension). Instead, the martensite grows as an alternating arrangement of the two variants. The reason for

including dissipation stems from the recognition that the parent-product interface moves at near velocity of sound as suggested by the emission of AE signals. Associated with this movement, there is a dissipation which tends to relax the system towards local equilibrium. We include this through a Rayleigh dissipation functional [17]. We also include heterogeneous nucleation at defect sites by including an appropriate strain energy [18].

We have kept the model simple in an attempt to capture these seemingly different types of features by choosing the deviatoric strain $\varepsilon = [(\partial u_x)/(\partial x) - (\partial u_y)/(\partial y)]/\sqrt{2}$ as the order parameter where u_x and u_y are the two components of the displacement field. Further we consider a *2d* square-to-rectangle transition [19, 20]. The effect of the bulk and shear strains are included only in a phenomenological way through a long-range interaction.

The free-energy functional of our system with the order-parameter ε is written as

$$F\{\varepsilon(\vec{r})\} = F_L\{\varepsilon(\vec{r})\} + F_{LR}\{\varepsilon(\vec{r})\}, \tag{2.1}$$

where F_L is a local free-energy functional and F_{LR} is a nonlocal long-range term that describes transformation induced strain-strain interaction. In a scaled form, the local free-energy F_L is

$$F_L = \int d\vec{r}\left[f_l(\varepsilon(\vec{r})) + \frac{D}{2}(\nabla\varepsilon(\vec{r}))^2 - \sigma(\vec{r})\varepsilon(\vec{r})\right]. \tag{2.2}$$

where D and σ are in a scaled form. Here, $f_l(\varepsilon(\vec{r})) = \frac{\tau}{2}\varepsilon(\vec{r})^2 - \varepsilon(\vec{r})^4 + \frac{1}{2}\varepsilon(\vec{r})^6$ with, $\tau = (T - T_c)/(T_0 - T_c)$ being the scaled temperature. T_0 is the first-order transition temperature at which the free energy for the product and parent phases are equal, and T_c is the temperature below which there are only two degenerate global minima $\varepsilon = \pm\varepsilon_M$. The stress field $\sigma(\vec{r})$ in Eqn. 2.2 modifies the free-energy f_l in such a way that the austenitic phase is locally unstable leading to the nucleation of the product phase.

Effective long-range interaction between the transformed domains results due to the coupling with the other components of the strain order parameter [21, 22]. However, as our approach is phenomenological, we use a simple form that respects the invariance of f_l under $\varepsilon \to -\varepsilon$. Following Wang and Khachaturyan [23], we use a simple form that satisfies this requirement when represented in the Fourier space, as

$$F_{LR}\{\varepsilon\} = \frac{1}{2}\int d\vec{k} B\left(\frac{\vec{k}}{k}\right)\{\varepsilon^2(\vec{r})\}_k\{\varepsilon^2(\vec{r})\}_{k^*}, \tag{2.3}$$

where $\{\varepsilon^2(\vec{r})\}_k$ is the Fourier transform of $\varepsilon^2(\vec{r})$ and $\{\varepsilon^2(\vec{r})\}_{k^*}$ is its complex conjugate. The direction dependent kernel is taken to have the form $B(\frac{\vec{k}}{k}) = -\beta\theta(k-\Lambda)\hat{k}_x^2\hat{k}_y^2$, where $\hat{k}_x$ and $\hat{k}_y$ are the unit vectors in x and y directions that contains information about the habit plane directions. Thus, the favorable directions of growth of the product are along $[11]$ and $[1\bar{1}]$. (The step function $\theta(k-\Lambda)$ has been introduced to impose a cutoff on the range of the long-range interaction.) The constant β is the strength of the interaction. This kernel incorporates the effect of the interface in a simple way. We stress that this is only a simple choice and is not unique. Other kernels with similar orientation dependence will give similar results[24]. The real space picture of $B(\vec{k}/k)$ is similar to the long-range interaction of Kartha *et. al.* [4].

Thus, we start with the Lagrangian $L = T - F$, where F is the total free-energy and T is the kinetic energy associated with the system. The kinetic energy is given by

$$T = \int d\vec{r}\rho \left[\left(\frac{\partial u_x(\vec{r},t)}{\partial t} \right)^2 + \left(\frac{\partial u_y(\vec{r},t)}{\partial t} \right)^2 \right]. \tag{2.4}$$

Here ρ is the mass density. The dissipation associated with the rapid motion of the interface is represented by the Rayleigh dissipative functional [17], written entirely in terms of $\varepsilon(\vec{r})$ is given by $R = \frac{1}{2}\gamma \int d\vec{r} \left(\frac{\partial}{\partial t} \varepsilon(\vec{r},t) \right)^2$. To model the AE signals, we recall that the mechanism of generation of the AE signals is generally attributed to the sudden release of the stored strain energy. In plasticity, the production of AE signals is attributed to the abrupt motion of the dislocations. The associated energy of AE signals, $E_{ae}(r)$ is taken to be proportional to $\dot{\varepsilon}^2(r)$, where $\dot{\varepsilon}$ is the local plastic strain rate [25]. This clearly has the same form as the Rayleigh dissipation functional [17]. Thus, while comparing results of the statistics of AE bursts, we need to simply compute $R(t)$.

We derive the equations of motion for ε using the equations of motion for the displacement fields given by

$$\frac{d}{dt}\left(\frac{\delta L}{\delta \dot{u}_i} \right) - \frac{\delta L}{\delta u_i} = -\frac{\delta R}{\delta \dot{u}_i},\ i = x,y. \tag{2.5}$$

The equation of motion for the deviatoric strain $\varepsilon(\vec{r},t)$ is given by

$$\frac{\partial^2}{\partial t^2}\varepsilon(\vec{r},t) = \nabla^2 \left[\frac{\partial f(\vec{r},t)}{\partial \varepsilon(\vec{r},t)} - \sigma(\vec{r}) - \nabla^2 \varepsilon(\vec{r},t) + \gamma \frac{\partial}{\partial t}\varepsilon(\vec{r},t) + 2\varepsilon(\vec{r},t) \int d\vec{k} B(\vec{k}/k) \{\varepsilon^2(\vec{k},t)\}_k e^{i\vec{k}.\vec{r}} \right], \tag{2.6}$$

Here, both β and γ are to be taken as rescaled parameters. The structure of Eqn. 2.6 is similar to that derived in [15] for 1-d except for the long-range term.

3. NUMERICAL SIMULATIONS

Simulation were carried out by discretizing Eqn.2.6 on a $N \times N$ grid using the Euler's scheme with periodic boundary conditions. The mesh size of the grid is $\Delta x = 1$ and the smallest time step $\Delta t = 0.002$. Most results reported here correspond to $N = 128, 256$. A pseudo-spectral technique is employed to compute the long-range term [26]. In all simulations reported in the paper, the cutoff Λ in the long-range expression defined in Eq. 2.3 is chosen to be 0.2. The inhomogeneous stress field $\sigma(\vec{r})$ is appropriately chosen to describe the defect configuration (see below). We consider two situations corresponding to the nucleation at a single- defect site and at several defect sites.

3.1 Nucleation at a Single-Defect Site

Consider the nucleation and growth of domains under a single quench, starting from the austenite phase to the martensite phase. In general, the stress field due to several defects located at $\vec{r}_j$ can be described by $\sigma(\vec{r}) = \sum_j^{j_{max}} \sigma_0(\vec{r}_j) exp\left(\frac{-|\vec{r}-\vec{r}_j|^2}{\zeta_j^2} \right)$, where $\sigma_0(\vec{r}_j)$ is the magnitude of the stress field at sites $\vec{r}_j$ which are randomly chosen defect sites, j_{max} is the total number of defect sites, and ζ_j is the width of the field.

We first consider a single isotropic defect with its core located at the center of the system. For a single-defect case, $\vec{r}_j = \vec{r}_0$. We choose $\zeta = 1$ and $\sigma_0 = 0.3$. With this value of σ_0, the system

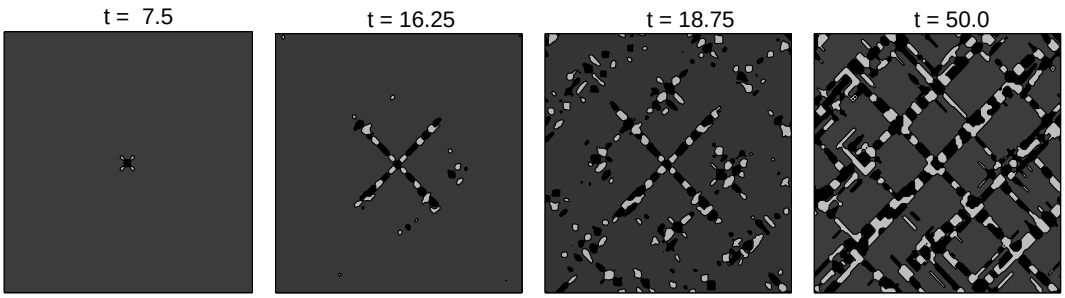

Figure 1: Morphological evolution for nucleation at a single- defect with $\beta = 50$, $\gamma = 4$ and $\tau = -2.0$. Grey cells correspond to the austenite phase and the black and the white to the two martensite variants.

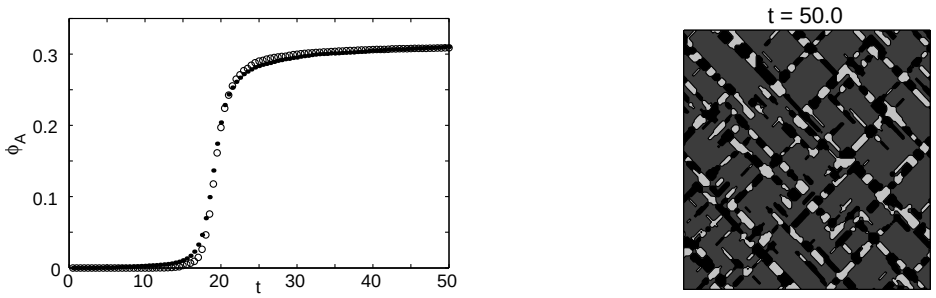

Figure 2: (a) Plot of the transformed area fraction ϕ_A with respect to time for N=128, $\beta = 50$, $\gamma = 4$,and $\tau = -2.0$. $\circ$ correspond to single-site case and $\bullet$ corresponds to the multi-site defect case. (b) Final morphological snapshot for multi-defect case with defect density 0.1% for $\beta = 50$, $\gamma = 4$ and $\tau = -2.0$

becomes locally unstable at the core $\vec{r}_0$. The parameters chosen for the simulations are $\beta = 50$ and $\gamma = 4$. At $t = 0$, we start with $\varepsilon(\vec{r},0)$ distributed in the interval $[-0.005, 0.005]$ representing the austenite phase and simultaneously 'turn on' the stress field $\sigma(\vec{r})$ as we quench the system to $\tau = -2.0$.

Figure 1 shows the nucleation and growth of the martensite domains from the defect core at various instants of time. (Grey regions represent the austenite phase $\{\varepsilon = 0\}$, black and white regions represent the two variants of martensite, $\{\varepsilon = \pm\varepsilon_{eq}\}$.) In a short time after quench ($t \sim 7.5$), a small nucleus emerges with $\varepsilon = \varepsilon_{eq}$. In addition, we also see the emergence of domains of the other variant ($\varepsilon = -\varepsilon_{eq}$) adjacent to the nucleus in the $[11]$ and $[1\bar{1}]$ directions. The twinned array propagate along $[11]$ and $[1\bar{1}]$ directions. (see Fig. 1, $t = 16.25$). A new set of nuclei ($\varepsilon = \varepsilon_{eq}$) are seen to be created at a finite distance from the propagating arrays. In course of time, several additional nuclei are created at finite distances from the original propagating fronts (see snap shot at $t = 18.5$). This can be attributed to the accumulation of long-range stress fields at these sites. These new nuclei give birth to secondary fronts that also propagate along $[11]$ and $[1\bar{1}]$. These observations in our simulation are in accordance with the collective nucleation mechanism discussed in [23] and the experiments by Ferraglio and Mukherjee [9]. The morphological evolution eventually stops beyond $t = 50$.

Figure 2a, shows the corresponding evolution of the area fraction ϕ of the martensitic phase ($\circ$). The transformation is seen to start around $t \sim 15$. The fraction increases sharply till about

$t \sim 20$, beyond which it saturates to a value close to 0.31. The spurt in the growth between $t = 15$ and 20 roughly coincides with the creation of the first set of additional nuclei.

3.2 Nucleation at Several Defect Sites

For the more realistic case of nucleation occurring at several defect sites, we choose $j_{max} = 16$ (nearly 0.1% of the total number of sites and N =128) and consider $\sigma_0(\vec{r}_j)$ to be uniformly distributed in the interval $[-0.3, 0.3]$. All other parameters are same as that for the single-defect case. Initially, $\varepsilon(\vec{r}, 0)$ is taken to be uniformly distributed in the interval $[-0.005, 0.005]$. At $t = 0$, we turn on the stress-field $\sigma(\vec{r})$. As in the case of single- site nucleation, around $t = 15$, nucleation of the product phase is seen to occur at several sites. By $t = 17.5$, these nuclei grow into twinned lenticular shape. Several additional nuclei emerge at finite distance from these original domains. These new sites at which the product phase nucleates most often coincides with the pre-existing defect sites. However, occasionally, nucleation does occur at sites where there were no defects due to stress accumulation arising from the long-range term, as in the case of single-site nucleation. There is a rapid growth of the product phase along $[11]$ and $[1\bar{1}]$ directions forming a criss-cross pattern of the martensite domains saturating by $t = 50$. A comparison of this final configuration, Fig. 2b with the corresponding single-site nucleation, Fig. 1d shows that the final morphologies are very similar implying that the morphology evolution is independent of the original defect configuration. Figure 2a also shows the time evolution of the area fraction ϕ for multi-defect case (•) which is very similar to the single-defect case.

3.3 Thermal Cycling and Hysteresis

We have performed 'continuous cooling' and 'heating' computer simulations where we change τ at a constant rate: the interval $\tau = 40$ to -80 is cooled in 1000 time steps. Using the same initial conditions as the single quench situation, we have monitored both the morphology and the area fraction of the transformed phase for single-defect nucleation as well as multi-defect nucleation case with several system sizes (N=128,256). The initial condition for the reverse transformation is the final configuration obtained during the cooling run.

Figure 3 shows the variation of the area fraction ϕ_A with τ for the heating and the cooling runs for the single defect (•) and multi defect cases (○) for $N = 128$. As can be seen, the difference between the hysteresis cycles corresponding to these two cases is negligible.

We have followed the morphological evolution of the martensitic domains both for the single and multi-defect cases. Here, we discuss multi-defect case only. Figure 4 shows the snap shots of the pattern at specifically chosen values of τ as the system is taken through a cycle. The snapshot at $\tau = -3.5$ shows the nucleation of martensitic domains at multiple locations. As the system is further 'under-cooled,' not only does these twins propagate in the $[11]$ and $[1\bar{1}]$ directions, the thickness of the martensite domains also increases. Further under-cooling shows that the twin width further increases. A late stage snap shot at $\tau = -45.5$ corresponding to $\phi \sim 90\%$ is shown. For the heating cycle, the final configuration of the cooling run is taken as the initial configuration and the austenite phase appears around $\tau \sim -22$. As τ is further increased, the martensite phase can be seen to be gradually disappear in the snapshots corresponding to $\tau = -5$ and 13. The overall final stage morphology of the heating run is very different from the initial stages of the cooling run.

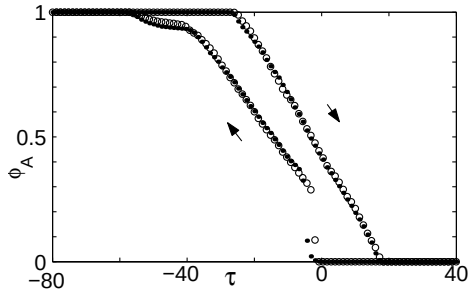

Figure 3: Area fraction of the transformed phase ϕ_A as a function of τ for both single defect ($\circ$) and multi-defect ($\bullet$) nucleation cases. The parameter values are $\beta = 50, \gamma = 4$ and $N = 128$. The defect density in multi-defect is 0.1% of sites.

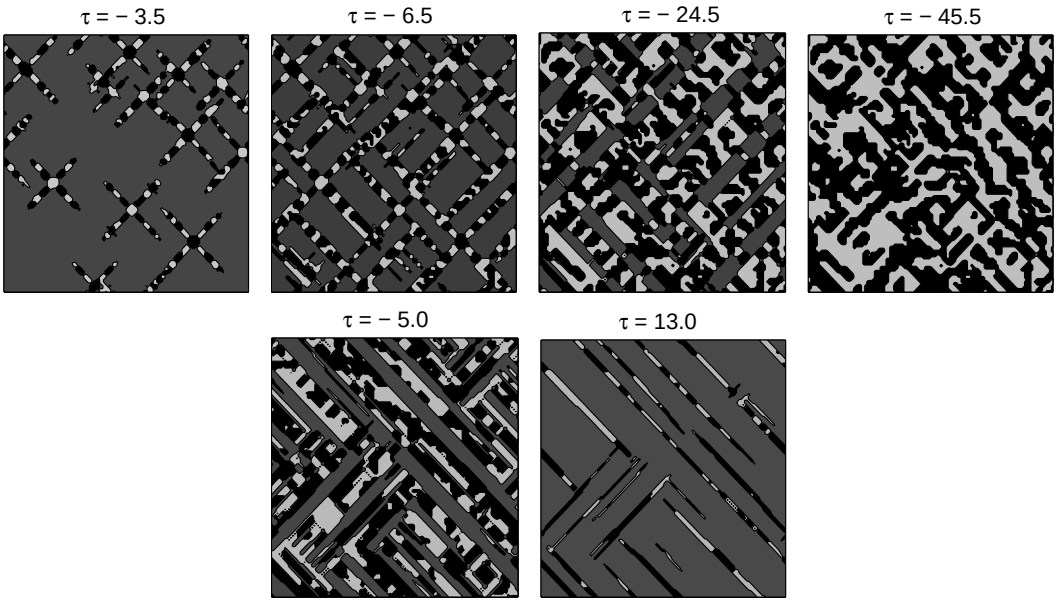

Figure 4: Morphological evolution during a cooling and heating cycle. The parameter values are $\beta = 50, \gamma = 4$ and $N = 128$ with a defect density 0.1% of the sites.

Thus, in our model, there is no long term memory effects, though there is short term memory as will be shown later.

3.4 Power Law Statistics During Thermal Cycling

From Fig. 3, it appears that changes in ϕ_A are smooth, but in reality, on a finer scale, the changes in ϕ_A are jerky. In fact, in experiments, thermal cycling is accompanied by the emission of acoustic energy in the form of bursts, a feature that reflects the jerky nature of the transformation. In the model, as mentioned earlier, the energy of acoustic signals is captured by the rate of energy dissipated given by $R(t) = -dE/dt$. We have calculated $R(t)$ during the heating and cooling runs.

Since, in experiments one finds that the AE signals show a power law statistics, we have investigated the distributions $D(R_A)$ of the amplitudes R_A of the AE signals and $D(\Delta t)$ of their durations Δt. $D(R_A)$ of R_A exhibits a power law $D(R_A) \sim A^{-\alpha_R}$ with an exponent α_R as shown in

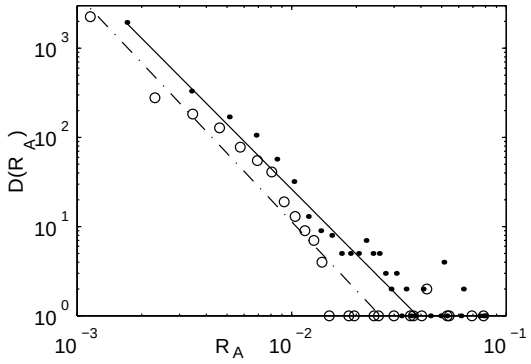

Figure 5: Log-log plot of $D(R_A)$ as a function of R_A. The parameter values are $\beta = 50, \gamma = 4$ and $N = 256$. The defect density in multi-defect is 1% of sites. [○ corresponds to single-defect case and • corresponds to multi-defect case.]

Fig. 5. Both single and multi-site cases exhibit the same exponent value $\alpha_R \sim 2.5$ over three orders in $D(R_A)$. As in experiments, the distribution $D(\Delta t)$ of the durations Δt of energy bursts also show a power law $D(\Delta t) \sim \Delta t^{-\tau_R}$ with an exponent value $\tau_R \approx 3.2$, for both the single and multi defect cases, although, the scaling regime is not as impressive as for R_A. We have also calculated the conditional average $< R_A >_c$ for a given value of Δt [27]. This is expected to obey a power law given by $< R_A >_c \sim \Delta t^{x_R}$. The value we get is about $x \approx 1.36$ for both these single and multi defect nucleation cases. Using these values, we find that the scaling relation $\alpha = x(\beta - 1) + 1$ is satisfied quite well. We have also carried out a similar analysis on $R(t)$ for the heating run.

The origin of the power law statistics in the model can be traced to the fact that we have included important ingredients of SOC dynamics, namely, the threshold dynamics, dissipation, the generation of large number of metastable states during the transformation, and a relaxation mechanism for the stored energy. The relaxation of the stored energy occurs at very fast time scales comparable to time scale of the speed of sound. Compared to this the driving force generated by thermal cycling increases with temperature slowly which is one of the characteristic features of SOC dynamics. Another important feature of the model, as also that of SOC dynamics, is the creation of large number metastable states during cooling or heating runs. This is a direct consequence of an interplay between the local free energy (free energy barrier) and the long-range interaction between the transformed domains. The free energy surface at any given time is a complex terrain of local barriers (metastable states). It must be noted that these local thresholds are *self generated* (transformation induced). At a given time, these local thresholds must be overcome by the increase in the driving force arising from the slow cooling (or heating) and once a local barrier is overcome, part of the driving force goes in creating a new twin and the rest is dissipated in the form of burst of energy due to the advancing one or more interfaces. The fact that long-range interaction is at the root of creating the local thresholds is further supported by the fact that we find a power law distribution even in the single- site nucleation case. (See • in Fig. 5.) The presence of defect sites only serves to trigger the initial nucleation process.

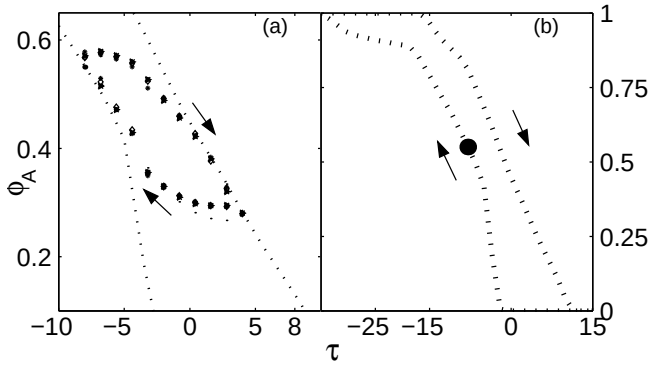

Figure 6: (a).Area fraction ϕ during thermal cycling in the interval $\tau = -8$ to 4 for cycles 1 (○),2 (Λ), 3 (•),4 (▷). (b)Hysteresis for the full cycle from the austenite to the martensite phase and back. (•) is the starting point of the small thermal cycles.

4. Shape Memory Effect

4.1 Correlated behavior of AE signals

In contrast to the scale free nature of correlation discussed above, a highly correlated behavior of AE signals is observed when the system is subjected to thermal cycling in a small temperature interval. To verify if this result can be captured by our model, consider the system being cooled from the austenite phase to a point in the martensite phase where a desired amount of martensite phase has developed. Starting from an appropriate point (shown as • in Fig. 6b, here chosen to be $\phi \sim 0.58$ in the full thermal cycle), we subject the system to repeated thermal cycling in a small temperature range $\tau_{min} = -8$ and $\tau_{max} = 4$. As in the case of full thermal cycling, for the small heating cycle also, the final configuration attained at $\tau_{max} = 4$, is taken as the initial configuration for the cooling run. For the present calculation, we have used $\beta = 35$ and $\gamma = 4$. Other parameter values are $\Lambda = 0.2, \zeta = 1$ and $N = 128$. During the first few cycles, the loops in the area fraction ϕ verses τ drift slightly, but stabilize after a first few cycles, here, after the sixth cycle. The first few cycles play the role of the *training* period known in experiments. After these first few cycles the system eventually circulates in the same set of configurations as we will show.

During the training cycles, the energy dissipated $R(t)$ evolves continuously, stabilizing only after the training period. A plot of $R(t)$ for several forward and reverse cycles (seventh to tenth) after stabilization is shown in Fig. 7. It is clear that the energy bursts (which mimic the AE signals), as in experiments [28, 29], exhibit a near repetitive pattern in time (temperature) during successive heating and cooling parts of the cycles.

4.2 Connection to shape memory effect

Simultaneous monitoring of the morphology shows that there is a correspondence between $R(t)$ and the changes in the spatial configuration of the martensite domains. The morphology changes drastically during the first few cycles. The domain configurations at the beginning of first few cycles are shown in Fig. 8. Figure 8a is the starting morphology for the first cycle that has been obtained by slowly cooling from the austenite phase. Figure 8d is that obtained at the end of sixth

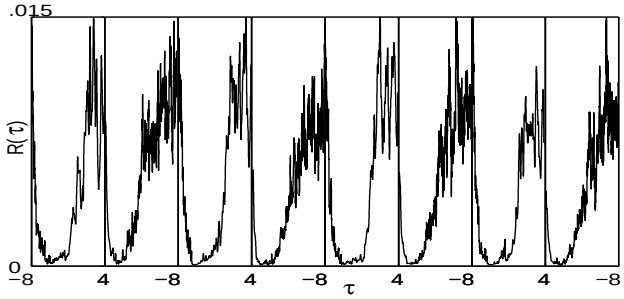

Figure 7: Repetitive nature of $R(\tau)$ for cycles 7 to 10.

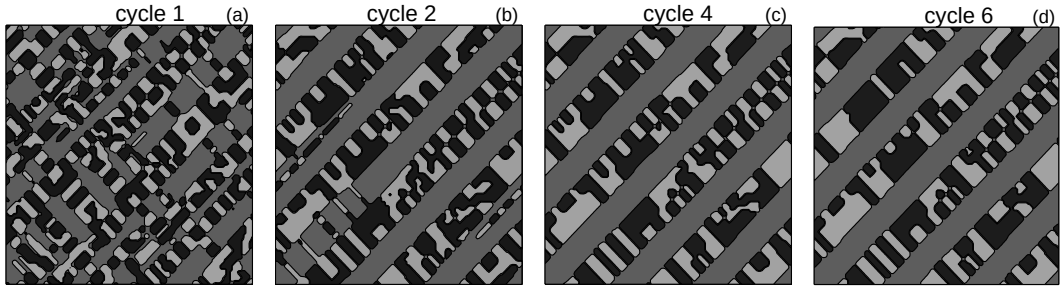

Figure 8: Morphology of the initial configurations at $\tau = -8.0$ for the first, second, fourth and the sixth thermal cycles.

cycle. As can be seen, most of the curved twin interfaces in the initial configuration (Fig. 8a) are rendered straight and several small twins coalesce to form a single variant of the same type. Further some regions of the austenite phase separating the martensite domains are washed out. Subsequent cycles are less effective. After the sixth cycles very little changes could be detected.

One should anticipate the repetitive nature of $R(t)$ are related to the changes in the microstructure within one thermal cycle. The snapshots of the morphology during one such stabilized cooling and heating cycle, the seventh one, (starting from the initial configuration shown in Fig. 8d) at selected intervals is displayed in Fig. 9. It is clear that during heating, the martensite domains shrink, opening up the austenite phase and some martensite domains even disappear. However, during cooling these domains reappear and the eventual morphology at the end of the cycle is practically recovered. As can be seen, the final configuration obtained during the seventh cycle, *Fig. 9d can be seen to be practically the same as Fig. 8d which is the initial configuration for the seventh cycle.* These observations are consistent with that observed in experiments [8].

To understand the repetitive nature of the energy bursts and the reversal of the morphology under thermal cycling, we need to understand the role played by the training cycles. Indeed, the repetitive pattern of the energy bursts during successive cycles (after the training period) is an indication that the system traverses through the same set of metastable states. From Fig. 8a, we note that the initial configuration for the first cycle has a large number of small domains compared to the configuration obtained after the sixth cycle shown in Fig. 8 d. In addition, the twin interfaces of Fig. 8a are rough. Such configurations are generally expected to have higher energy compared to straighter ones. During the first few cycles, the free energy landscape is so modified that it

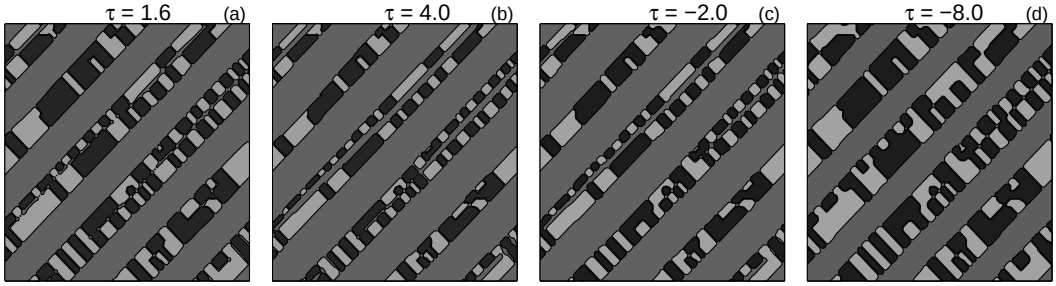

Figure 9: Sequential morphological snapshots for $\tau = 1.6(a), 4.0(b), -2.0(c), -8.0(d)$ during the seventh cycle. The initial configuration for the cycle is that shown in Fig. 8(d).

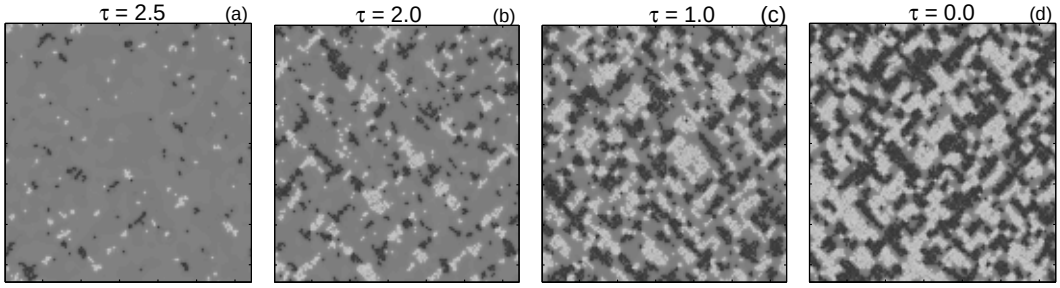

Figure 10: Development of Tweed like pattern

smoothen's out the energy barriers corresponding to large number of twin interfaces in Fig. (8a) with very little change in the area fraction. As in the case of power law distribution, a crucial role in smoothening process is actually played by the long-range interaction term, as the growth (shrinkage) of a martensite domain is influenced by the configuration of rest of the domains. To verify this, we have computed the free energy F_{LR} arising from the long-range interaction between the domains and find that it actually becomes more negative with successive cycles saturating after first few cycles. This additional contribution leads to a reduction in the local free energy, F_L, as well. The net effect is to create *a deeper set of metastable states for the system to circulate for the stabilized cycles*. Within one such stabilized cycles, say seventh, the starting configuration (Fig. 8d) has the lowest free energy reaching a maximum at the end of a heating cycle, ie., at $\tau = 4.0$, Fig. 9b. Thereafter it decreases during cooling. The increasing or decreasing width of the martensite domains as we decrease or increase the temperature is surprisingly similar to that observed in experiments. (See Fig. 12 of Ref.[8].)

5. Pretransitional effects

Now we consider the possibility of recovering pretransitional effects in our model. As mentioned in the introduction, the mechanism attributed by Kartha *et. al.* [4], is the dependence of the elastic constant on local disorder in composition. It is clear that once the basic mechanism is included, the model should lead to results similar to that in Kartha *et. al*. We shall adopt the same idea and assume that the transition temperature depends on local compositional fluctuations

through $T_0(\vec{r}) = T_0(\bar{c}) - A\delta c(\vec{r})$, where A is the relative strength of coupling to compositional fluctuations δc, assumed here to be randomly distributed. In scaled variable that we use, this leads to τ being replaced by $\tau = \tau(\bar{c}) + a\delta c$, where $\bar{c}$ is the average concentration and a is a scaled variable.

In our simulations, we assume that the initial concentration fluctuations, considered as frozen, are drawn from a normalized Gaussian. Here we just need to solve the equations of motion numerically for various values of τ and a. (We have varied a from 0.0 to 1.2.) The range of values of β and γ wherein we find the tweed structure is in the region of relatively low values. ($\beta < 20$ and $\gamma < 0.7$.) Here, we report results for $a = 0.9, \beta = 10$ and $\gamma = 0.1$. A typical set of morphologies are shown in Fig. 10. The pretransitional effects become noticeable even when $\tau = 4$. For $\tau = 2$ the directionality of the tweed pattern is already evident. As we decrease the temperature, this structure becomes more dominant. It must be mentioned here that in our case, these patterns do not change after reaching a steady state. Thus, we do not have the dynamic tweed structure reported by Kartha *et. al*. This is because, in our model the effect of temperature goes only in the local free energy and there are no thermal fluctuations. We also note that the pretransitional effects are pronounced when both β and γ are small. However, we note that including the changes in the transition temperature on local disorder is somewhat similar to the contribution from defects except that internal stresses (arising from deviations from the average concentration) are of much smaller magnitude compared to that due to defects.

6. SUMMARY AND DISCUSSIONS

The paper summarizes the results of a comprehensive study of the dynamics of strain driven martensitic transformations within the framework of a two dimensional square-to-rectangle transition. Due to the fact that the long-range term is introduced phenomenologically, the model should be viewed as a model whose primary aim is to capture the essential physics of the transformations. We however note that it includes all the important contributions arising from different mechanisms in a transparent way. In doing so, we are able to study the dynamics of the strain driven transition that explains the three unusual features of the martensitic transformation that were sought to be modeled. The first important feature that emerges from the model is the fact that the elastic energy stored is released in the form of bursts. (Note that we have also established a correspondence between the dissipative functional and the energy of AE signals.)

Second, the model provides a proper basis to explain the power law statistics of the AE signals observed in experiments. The power law statistics arises due to the fact that we have included threshold dynamics, dissipation, the generation of large number of metastable states during the transformation, and a relaxation mechanism for the stored energy whose time scale is much faster than the time scale of the drive force. It is interesting to point out that both cases of single-defect and multi-defect nucleation lead to power laws strongly suggesting that quenched defects do not play any role in the power law. The model also predicts the near repetitive bursts of energy under successive thermal cycles in a small temperature interval as observed in experiments on acoustic emission [8, 29, 28]. This comes as a surprise as the nature of correlation in the latter case is 'periodic' in contrast to the scale free nature of correlations discussed in the power law statistics of AE signals. More importantly, these bursts of energy have been shown to be correlated to the growth and shrinkage of martensite plates. The underlying cause of the correlated nature of

AE signals and reversal of the morphology during successive cycles after the training cycles has been traced to the influence of the long-range interaction term. The role of training cycles is also elucidated. During the training period the long-range term has a tendency to smoothen out higher energy barriers in the free energy landscape which induces a transformation pathway along a unique set *of low energy metastable configurations*. Finally, it is not surprising that the model also reproduces tweed like features.

It is interesting to note the similarity of morphological patterns with real micrographs. Patterns studied in the context of single-defect and multi-defect nucleation show that the eventual morphology are independent of the the original defect configuration. It is not clear if this is true of real systems although experiments of Vives *et. al.*, [5] provide an indirect evidence. In addition, the model shows hysteresis under thermal cycling. Even though, the model explains several generic features stated above, we stress that our model is not material specific.

As mentioned the pretransitional effect is pronounced when both β and γ values are small. The low values of γ is physically understandable as one expects that there would be hardly any dissipation in the high temperature phase where there are no martensite domains. The smallness of β is also understandable physically (as the magnitude of fluctuations in the composition is not high). However, the value of β cannot be determined in terms of the elastic constants as in the case where the kernel is derived by using the compatibility relation [4].

References

[1] S. Muto, S. Takeda, R. Oshima, and F. E. Fujita, J. Phys.: Condens. Matter **1**, 9971 (1989).

[2] R. Oshima, M. Sugiyama and F. E. Fujita, Metall. Trans A, **19A**, 803 (1988).

[3] I.M. Robertson and C. M. Wayman, Phil. Mag A, **48**, 421 (1983); *ibid* **48**, 443 (1983); *ibid* **48**, 629 (1983).

[4] Sivan Kartha, J. A. Krumhansl, J. P. Sethna, and L. K. Wickham, Phys. Rev. B **52**, 803 (1995).

[5] E. Vives, J. Ortín, L. Mañosa, I. Ràfols, R. Pérez- Magrané and A. Planes, Phys. Rev. Lett. **72**, 1694 (1994).

[6] E. Vives, I. Ràfbs, L. Mañosa, J. Ortín and A. Planes, Phys. Rev. B **52**, 12644(1995); See also, Ll. Carrillo, Ll.Mañosa, J. Ortín, A. Planes, and E. Vives, Phys. Rev. Lett. **81**, 1889 (1998).

[7] P. Bak, C. Tang, and K. Wiesenfeld, Phys. Rev. A **38**, 364 (1988);

[8] F. C. Lovey and V. Torra, Prog. Mater. Sci. **44**, 189 (1999).

[9] P. L. Ferraglio and K. Mukherjee, Acta Metall **22**, 835(1974).

[10] J. W. Brooks, M. H. Loretto and R. E. Smallmann, Acta Metall. **27**, 1829 (1979).

[11] A. G. Khachaturyan, *Theory of Structural Tranformations in Solids* (Wiley, New York).

[12] R. Ahluwalia and G. Ananthakrishna, Phys. Rev. Lett. **86**, 4076 (2001).

[13] S. Sreekala and G. Ananthakrishna, Phys. Rev. Lett. bf 90, 135501-1 (2003).

[14] S. Sreekala, R. Ahluwalia, and G. Ananthakrishna, Phys. Rev. B **70**,224105 (2004).

[15] G. S. Bales and R. J. Gooding, Phys. Rev. Lett. **67**, 3412(1991).

[16] A. C. E. Reid and R. J. Gooding, Phys. Rev. B **50**, 3588(1994).

[17] L. D. Landau and E. M. Lifschitz, *Theory of Elasticity*, 3rd ed.(Pergamon, Oxford, 1986).

[18] W. Cao, J. A. Krumhansl and R. J. Gooding, Phys. Rev. B **41**, 11319 (1990).

[19] J. A. Krumhansl, Solid State Commun. **84**, 251(1992).

[20] A. E. Jacobs, Phys. Rev. B **31**, 5984 (1985).

[21] S. Kartha, T. Castan, J. A. Krumhansl and J. P. Sethna, Phys. Rev. Lett. **67**, 3630 (1991).

[22] S. R. Shenoy, T. Lookman, A. Saxena and A. R. Bishop, Phys. Rev. B **60**, R12537 (1999).

[23] Y. Wang and A.G. Khachaturyan, Acta Mater. **45**, 759(1997).

[24] This choice is not unique. Further, it may be possible to derive an appropriate kernel which couples bilinear terms in $\varepsilon(r)$ and $\varepsilon(r')$. However, we expect that the functional form of $B(\vec{k}/k)$ would be complicated.

[25] J. Weiss, F. Lahaie, and J. R. Grasso, J. Geo. Research, **105**, 433 (2000).

[26] C. Sagui and R. C. Desai, Phys. Rev. E, **49**, 2225 (1994).

[27] I. Rafols and E. Vives, Phys. Rev. B **52**, 12651 (1995).

[28] A. Amengual, Ll. Mañosa, F. Marco, C. Picornell, C. Segui, and V. Torra, Thermochim. Acta **116**, 195 (1987).

[29] C. Picornell, C. Segui, V. Torra, F.C. Lovey, and R. Rapacioli, Thermochim. Acta **113**, 171 (1987).